Supplement C to "Evaluated kinetic and photochemical data for atmospheric chemistry: Volume VII - Criegee intermediates":

Ambient calculations for representative conditons in the south-east UK

Contents

C1. Introduction **1**

C2. Input data **1**

C3. Results **4**

C4. Uncertainties **14**

References **15**

C1. Introduction

The kinetics and mechanistic information for sCI reactions recommended in the present evaluation provides the basis for representing the associated impact of alkene ozonolysis in atmospheric chemical mechanisms. The significance of sCIs as atmospheric oxidants can be discussed in terms of Eq. (1), which defines the steady state concentration of a given stabilised Criegee intermediate, [sCI_i], maintained by a balance between production and loss:

$$[\mathrm{sCI_i}] = \frac{\sum_j (Y_{ij} \times k_{1j} \times [\text{alkene}_j] \times [\mathrm{O_3}])}{(k_{di} + J_i + k_{2i}[\mathrm{H_2O}] + k_{3i}[(\mathrm{H_2O})_2] + k_{4i}[\mathrm{SO_2}] + k_{5i}[\mathrm{NO_2}] + \cdots + \cdots)} \quad (1)$$

Here, k_{1j} is the rate coefficient for the reaction of O_3 with alkene$_j$, and Y_{ij} is the yield of sCI_i from that reaction. The numerator of Eq. (1) therefore quantifies the source term for formation of sCI_i from all relevant alkenes, and the denominator quantifies the sum of the rates of the unimolecular and individual bimolecular loss processes for sCI_i, with the example contributors to the summation being based on the processes shown in Fig. 1 of the main paper.

The production rates, loss rates and steady-state concentrations of a series of sCIs have been calculated for average ambient conditions representative of the south-east UK, based on data for three national monitoring stations. These consider averaged winter and summer conditions at each of a rural background, suburban background and urban kerbside (or urban traffic) location.

C2. Input data

Information on the sites included in the present analysis, and the associated observational data, is sumarised in Table 1. The sites are part of both the "Automatic Urban and Rural Network (AURN)" and the "Automatic Hydrocarbon Network" set up by the UK Department for Environment, Food and Rural Affairs (Defra). The data for O_3, NO_2, SO_2, modelled temperature, C_1-C_5 alkenes and isoprene were obtained from the national data archive at the UK-AIR Air Information Resource (http://uk-air.defra.gov.uk/). As also indicated in Table 1, the hydrocarbon data were supplemented by additional information for 2-methylpropene, α-pinene, and limonene (Whalley et al., 2018) and HC(O)OH (Bannan et al., 2017) from the Clean Air for London (ClearfLo) project, and a distribution of C_5 and C_6 alkenes inferred from the National Atmospheric Emissions Inventory (NAEI) speciation (Goodwin et al., 2001; Utembe et al., 2005). The relative humidity values were based on data for London Heathrow airport, as presented by Brimblecombe (2013). It is emphasized that all the applied data are average values appropriate for the three-month winter and summer periods, within which there can be considerable diurnal and day-to-day variability.

The kinetics and mechanistic information describing sCI formation and removal was taken primarily from the current evaluation, supplemented by additional information where necessary. The kinetics of the reactions of O_3 with C_1-C_4 alkenes, isoprene, α-pinene and limonene, and the associated sCI yields, were therefore taken from the present work. The kinetics of the reactions of O_3 with buta-1,3-diene and the C_5 and C_6 alkenes were taken from the recent evaluation of McGillen et al. (2020), with the associated sCI yields based on information from a variety of sources, as summarized in Table 2.

Based on the information presented and discussed in Sects. 6 and 7 of the main review, sCI removal by unimolecular decomposition and bimolecular reactions with H_2O, $(H_2O)_2$, NO_2, SO_2 and HC(O)OH was represented. For CH_2OO, *E*- CH_3CHOO, *Z*-CH_3CHOO, $(CH_3)_2COO$, and the C_4 isoprene-derived intermediates (*E*- and *Z*-$(CH{=}CH_2)(CH_3)COO$ and *E*- and *Z*-$(C(CH_3){=}CH_2)CHOO$), the kinetic data were taken from the current evaluation. Where only a 298 K recommendation is made for a unimolecular decomposition rate coefficient (i.e. for CH_2OO and *E*-CH_3CHOO), the applied temperature dependence was based on that calculated by Vereecken et al. (2017), with the 298 K value for CH_2OO set at half the recommended upper limit. Where only an upper limit recommendation is made for bimolecular reactions (i.e. the reactions of H_2O and $(H_2O)_2$ with *Z*-CH_3CHOO and $(CH_3)_2COO$), these were assumed to be uncompetitive; this being consistent with the very low rate coefficients calculated theoretically (Vereecken et al., 2017).

The rate coefficients for the reactions of the higher alkyl-substituted sCIs, formed from the C_5 and C_6 alkenes (identified in Table 3), were taken to be the same as those for the corresponding methyl-substituted species (i.e. *E*-CH_3CHOO, *Z*-CH_3CHOO or $(CH_3)_2COO$); and those for the unsaturated C_3 species formed from buta-1,3-

Table 1. Summary of conditions and input parameters used for representative ambient calculations.

	Chilbolton Observatory		London Eltham		London Marylebone Rd		Comment
Site type	Rural Background		Suburban Background		Urban Traffic		
Location	51.149617, -1.438228		51.452580, 0.070766		51.522530, -0.154611		
	Winter	Summer	Winter	Summer	Winter	Summer	(a)
Temperature (K)	277.6	288.2	278.0	290.4	277.8	290.2	(b),(c)
Relative humidity	85 %	70 %	85 %	70 %	85 %	70 %	(d)
O_3 (ppbv)	26.0	28.5	17.7	26.5	7.4	12.9	(b)
NO_2 (ppbv)	6.2	3.0	12.9	5.7	36.0	31.1	(b)
SO_2 (ppbv)	0.36	0.28	1.8 [e]	1.2 [e]	1.8	1.2	(b)
HC(O)OH (ppbv)	0.043	0.89	0.12	0.91	0.63	1.3	(f)
ethene (pptv)	692.7	302.4	1163.7	389.8	2475.1	1718.8	(b)
propene (pptv)	106.9	60.5	282.4	150.3	735.9	428.3	(b)
but-1-ene (pptv)	47.5	45.8	48.1	31.1	106.8	102.0	(b)
trans-but-2-ene (pptv)	16.6	16.2	32.2	20.2	56.8	154.1	(b)
cis-but-2-ene (pptv)	17.0	18.9	23.1	17.3	25.1	67.9	(b)
2-methylpropene (pptv)	40.2	38.7	40.7	26.3	90.4	86.3	(g)
buta-1,3-diene (pptv)	40.4	42.9	32.2	21.1	32.2	16.0	(b)
pent-1-ene (pptv)	9.3	8.4	14.9	13.7	28.4	23.0	(b)
trans-pent-2-ene (pptv)	5.1	4.6	18.1	12.1	34.3	38.9	(b)
cis-pent-2-ene (pptv)	4.5	4.1	10.3	8.0	19.6	19.3	(h)
2-methylbut-1-ene (pptv)	1.8	1.6	4.1	3.2	7.9	7.8	(h)
2-methylbut-2-ene (pptv)	3.4	3.1	7.8	6.1	14.8	14.6	(h)
3-methylbut-1-ene (pptv)	2.3	2.1	5.2	4.1	10.0	9.8	(h)
hex-1-ene (pptv)	4.1	3.8	9.5	7.4	18.1	17.8	(h)
trans-hex-2-ene (pptv)	0.3	0.3	0.7	0.6	1.3	1.3	(h)
cis-hex-2-ene (pptv)	0.3	0.3	0.7	0.6	1.3	1.3	(h)
isoprene (pptv)	8.0	29.9 (8.5,21.4)	18.8	203.2 (12.5,190.7)	13.8	55.6 (6.8,48.8)	(b),(i)
α-pinene (pptv)	-	23.4	-	203.4	-	52.0	(j)
limonene (pptv)	-	8.0	-	70.0	-	17.9	(j)

Comments: [a] Winter averages based on data for January, February and December 2019; Summer averages based on data for June, July and August 2019; [b] Measured data from the Defra UK Automatic Urban and Rural Network (AURN) and UK Automatic Hydrocarbon Network, available from http://uk-air.defra.gov.uk/. Chemical species data reported in μg m^{-3} concentration units, derived from the measured mixing ratios for assumed reference ambient conditions of 20 °C and 101.3 kPa. For this analysis, the data were converted back to mixing ratios using reciprocal conversion factors; [c] Based on modelled meteorological data; [d] Representive values for south-east England, based on data presented by Brimblecombe (2013); [e] Major sources of SO_2 are power generation and industrial combustion. Mixing ratios at Eltham therefore assumed equivalent to those measured at Marylebone Road; [f] London Marylebone Road values based on data from the ClearfLo project (Bannan et al., 2017). Other values inferred from Marylebone data, with primary contributions scaled in proportion to NO_x level, and a constant summer background contribution at all sites; [g] 2-methylpropene mixing ratio inferred relative to but-1-ene mixing ratio using the hydrocarbon distribution measured at North Kensington (London) by Whalley et al. (2018) as part of the ClearfLo project; [h] Mixing ratios for a series of C_5 and C_6 alkenes inferred relative to those for pent-1-ene and *trans*-pent-2-ene using emitted speciation applied by Utembe et al. (2005), based on UK National Atmospheric Emissions Inventory (NAEI) data (Goodwin et al., 2001); [i] Isoprene mixing ratios are made up of anthopogenic and biogenic components. Winter measurements assumed to be entirely anthropogenic, and the winter isoprene/buta-1,3-diene ratios are used to infer the summer contributions (shown in brackets) for anthropogenic and biogenic isoprene, respectively (e.g. as described on pages 48-51 of AQEG, 2009); [j] Summer α-pinene and limonene mixing ratios inferred relative to biogenic isoprene mixing ratio using the hydrocarbon distribution measured at North Kensington (London) by Whalley et al. (2018) as part of the ClearfLo project.

Table 2. Identities of sCIs formed from ozonolysis of the considered alkenes, and their yields (Y_{sCI}). [a]

alkene	sCI	Y_{sCI}	alkene	sCI	Y_{sCI}
ethene	CH_2OO	0.42	2-methylbut-2-ene [f]	*E*-C_2H_5CHOO	0.064
propene	CH_2OO	0.2		*Z*-C_2H_5CHOO	0.064
	E-CH_3CHOO	0.05		$(CH_3)_2COO$	0.252
	Z-CH_3CHOO	0.05	3-methylbut-1-ene [d]	CH_2OO	0.193
but-1-ene	CH_2OO	0.137		*E*-*i*-C_3H_7CHOO	0.0485
	E-C_2H_5CHOO	0.0665		*Z*-*i*-C_3H_7CHOO	0.0485
	Z-C_2H_5CHOO	0.0665	hex-1-ene [c]	CH_2OO	0.227
trans-but-2-ene	*E*-CH_3CHOO	0.172		*E*-*n*-C_4H_9CHOO	0.0415
	Z-CH_3CHOO	0.258		*Z*-*n*-C_4H_9CHOO	0.0415
cis-but-2-ene	*E*-CH_3CHOO	0.253	*trans*-hex-2-ene [d]	*E*-CH_3CHOO	0.162
	Z-CH_3CHOO	0.127		*Z*-CH_3CHOO	0.244
2-methylpropene	CH_2OO	0.147		*E*-*n*-C_3H_7CHOO	0.086
	$(CH_3)_2COO$	0.063		*Z*-*n*-C_3H_7CHOO	0.128
buta-1,3-diene [b]	CH_2OO	0.141	*cis*-hex-2-ene [d]	*E*-CH_3CHOO	0.271
	Z-$(CH{=}CH_2)CHOO$	0.031		*Z*-CH_3CHOO	0.135
	E-$(CH{=}CH_2)CHOO$	0.068		*E*-*n*-C_3H_7CHOO	0.143
pent-1-ene [c]	CH_2OO	0.193		*Z*-*n*-C_3H_7CHOO	0.071
	E-*n*-C_3H_7CHOO	0.0485	isoprene [g]	CH_2OO	0.547
	Z-*n*-C_3H_7CHOO	0.0485		*E*-$(CH{=}CH_2)(CH_3)COO$	0.075
trans-pent-2-ene [d]	*E*-CH_3CHOO	0.120		*Z*-$(CH{=}CH_2)(CH_3)COO$	0.032
	Z-CH_3CHOO	0.181		*E*-$(C(CH_3){=}CH_2)CHOO$	0.031
	E-C_2H_5CHOO	0.088		*Z*-$(C(CH_3){=}CH_2)CHOO$	0.014
	Z-C_2H_5CHOO	0.131	α-pinene	*E*-pinonaldehyde-A-oxide	0.0324
cis-pent-2-ene [d]	*E*-CH_3CHOO	0.201		*Z*-pinonaldehyde-A-oxide	0.0162
	Z-CH_3CHOO	0.100		*E*-pinonaldehyde-K-oxide	0.0657
	E-C_2H_5CHOO	0.146		*Z*-pinonaldehyde-K-oxide	0.0657
	Z-C_2H_5CHOO	0.073	limonene	*E*-limononaldehyde-A-oxide	0.0486
2-methylbut-1-ene [e]	CH_2OO	0.158		*Z*-limononaldehyde-A-oxide	0.0243
	E-$(C_2H_5)(CH_3)COO$	0.061		*E*-limononaldehyde-K-oxide	0.099
	Z-$(C_2H_5)(CH_3)COO$	0.061		*Z*-limononaldehyde-K-oxide	0.099

Comments

[a] Except where commented, the total yields are based on those presented in Table 2 of the main review, with the speciation informed by the mechanistic information given in the corresponding data sheets in Supplement A; [b] Total yield based on that used in the Master Chemical Mechanism (http://mcm.york.ac.uk/); [c] Total yields based on the trend reported for alk-1-enes by Hasson et al. (2001); [d] Total yields based on the trend reported for symmetric internal alkenes by Hakala and Donahue (2018); [e] Total yield interpolated, based on consideration of yields for 2-methylpropene and β-pinene; [f] Total yield interpolated from the (identical) recommended yields for *cis*-but-2-ene and 2,3-dimethylbut-2-ene; [g] Total yield and distribution taken from the analysis in data sheet CGI_21 in Supplement B.

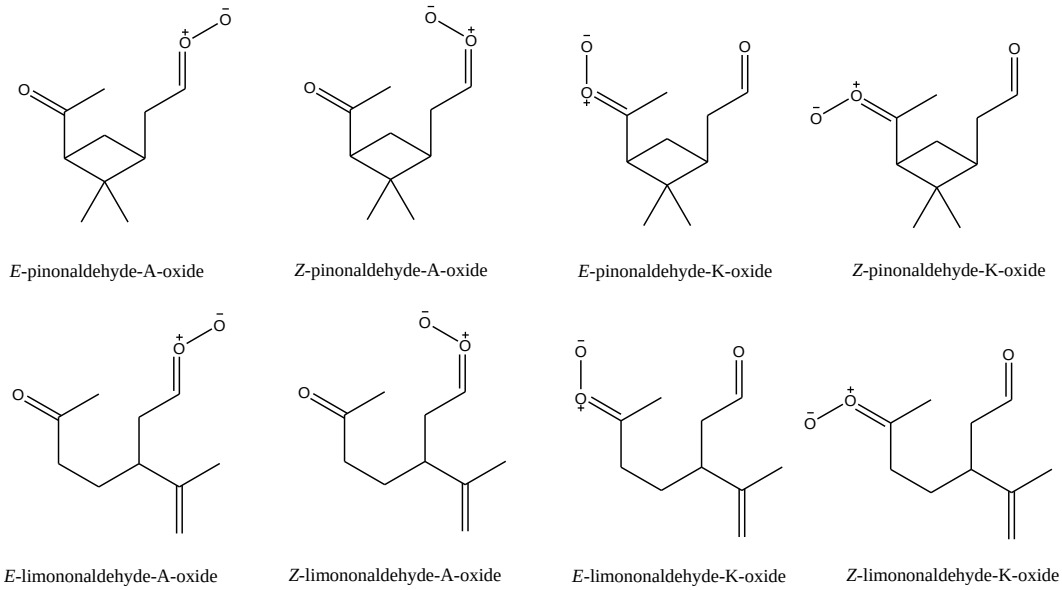

Figure 1: Structures of pinonaldehyde oxide and limononaldehyde oxide sCIs, formed from the reactions of O_3 with α-pinene and limonene.

---

diene (*E*- and *Z*-(CH=CH_2)CHOO) were based on those for the corresponding C_4 isoprene-derived species (i.e. *E*- and *Z*-(C(CH_3)=CH_2)CHOO). In the cases of the the C_{10} pinonaldehyde oxide and limononaldehyde oxide isomers formed from α-pinene and limonene (shown in Fig. 1), the rate coefficients for unimolecular decomposition and bimolecular reactions with H_2O and $(H_2O)_2$ were taken from the theoretical study of Vereecken et al. (2017). Those for the bimolecular reactions of NO_2, SO_2 and HC(O)OH with the (mono-substituted) "A" isomers were based on those for *E*- and *Z*-CH_3CHOO, and those for the (di-substituted) "K" isomers on $(CH_3)_2$COO.

C3. Results

Production rates: Fig. 2 shows the production rates for the considered set of sCIs for the representative winter and summer conditions at each of the sites. As indicated in Eq. (1), the relative production rate of a given sCI is determined by the concentrations of its precursor alkenes, the rate coefficients for the reactions of O_3 with each of those alkenes, and the associated yields of the sCI. As shown in Table 2, at least one of the core set of C_1-C_3 sCIs is generated from all the precursor alkenes, except α-pinene and limonene, and therefore the core set (shown towards the left of each panel in Fig. 2) collectively makes an important contribution to the total production rate in each case. The respective winter and summer contributions of the core set at each of the sites are 91 % and 75 % (Chilbolton Observatory); 88 % and 42 % (London Eltham); and 88 % and 85 % (London Marylebone Road). The reduced contributions in the summer result from an important contribution made by the α-pinene and limonene derived sCIs (see below).

Within the core set of C_1-C_3 sCIs, the formation of *E*- and *Z*-CH_3CHOO is most significant, because they are formed from propene and all the alk-2-enes in the speciation. They are also favoured because reaction with O_3 is a major (and sometimes the dominant) removal route for alk-2-enes (and other internal alkenes), by virtue of their particularly rapid reactions with O_3. CH_2OO also makes a notable contribution to the totals, because it is formed from all the alk-1-enes, including buta-1,3-diene and isoprene. The higher alkyl-substituted sCIs make systematically lower contributions, primarily because their precursor alkenes have systematically lower abundances. Thus, the respective production rates of *E*- and *Z*-C_2H_5CHOO, *E*- and *Z*-*n*-C_3H_7CHOO and *E*- and *Z*-*n*-C_4H_9CHOO are about one, two and three orders of magnitude lower than those of *E*- and *Z*-CH_3CHOO.

As indicated above, the sCIs formed from biogenic hydrocarbons logically make an increased and important collective contribution under the summer conditions, particularly at the London Eltham site. The higher abundance of biogenic hydrocarbons at London Eltham and the comparable abudances at Marylebone Road and the rural background site at Chilbolton Observatory, may appear counter-intuitive. However, this may be

Table 3. Summary of results.

	Chilbolton Observatory		London Eltham		London Marylebone Rd	
	Winter	Summer	Winter	Summer	Winter	Summer
sCI production rate (molecule cm^{-3} s^{-1})	6.34×10^4	8.70×10^4	8.77×10^4	2.42×10^5	6.67×10^4	2.17×10^5
sCI concentration (molecule cm^{-3})	386	375	536	1075	379	879
SO_2 oxidation rate (% h^{-1})	0.006	0.007	0.008	0.028	0.006	0.009
HC(O)OH oxidation rate (% h^{-1})	0.04	0.04	0.05	0.11	0.03	0.08
Contributions to total sCI loss						
Unimolecular decomposition	45.7%	49.3%	46.7%	57.7%	43.8%	49.0%
Reaction with H_2O	9.3%	9.6%	8.9%	8.6%	8.4%	9.3%
Reaction with $(H_2O)_2$	44.4%	38.2%	42.2%	29.1%	43.0%	37.0%
Reaction with SO_2	0.3%	0.2%	1.3%	1.6%	1.2%	0.6%
Reaction with NO_2	0.2%	0.1%	0.4%	0.1%	1.1%	0.6%
Reaction with HC(O)OH	0.2%	2.6%	0.5%	3.0%	2.4%	3.4%
Contributions to sCI speciation						
CH_2OO	1.36%	1.20%	1.21%	1.06%	1.57%	0.83%
E-CH_3CHOO	0.52%	0.39%	0.48%	0.14%	0.48%	0.418%
Z-CH_3CHOO	78.83%	58.06%	76.16%	24.47%	74.96%	76.99%
$(CH_3)_2COO$	7.12%	5.16%	7.28%	2.90%	8.13%	4.14%
Z-$(CH{=}CH_2)(CH_3)COO$	0.00%	0.01%	0.00%	0.01%	0.00%	0.00%
E-$(CH{=}CH_2)(CH_3)COO$	1.27%	3.03%	1.27%	6.10%	0.44%	0.90%
Z-$(C(CH_3){=}CH_2)CHOO$	0.00%	0.00%	0.00%	0.01%	0.00%	0.00%
E-$(C(CH_3){=}CH_2)CHOO$	0.15%	0.36%	0.15%	0.67%	0.06%	0.11%
E-C_2H_5CHOO	0.06%	0.04%	0.08%	0.02%	0.09%	0.04%
Z-C_2H_5CHOO	9.09%	6.44%	12.28%	4.14%	13.25%	7.29%
E-*n*-C_3H_7CHOO	0.00%	0.00%	0.00%	0.00%	0.01%	0.00%
Z-*n*-C_3H_7CHOO	0.65%	0.46%	0.64%	0.26%	0.68%	0.33%
E-*i*-C_3H_7CHOO	0.00%	0.00%	0.00%	0.00%	0.00%	0.00%
Z-*i*-C_3H_7CHOO	0.03%	0.02%	0.03%	0.02%	0.03%	0.02%
E-*n*-C_4H_9CHOO	0.00%	0.00%	0.00%	0.00%	0.00%	0.00%
Z-*n*-C_4H_9CHOO	0.09%	0.07%	0.10%	0.04%	0.11%	0.06%
E-$(C_2H_5)(CH_3)COO$	0.02%	0.02%	0.02%	0.01%	0.03%	0.02%
Z-$(C_2H_5)(CH_3)COO$	0.02%	0.02%	0.02%	0.01%	0.03%	0.02%
Z-$(CH{=}CH_2)CHOO$	0.01%	0.00%	0.00%	0.00%	0.00%	0.00%
E-$(CH{=}CH_2)CHOO$	0.76%	0.54%	0.26%	0.07%	0.14%	0.03%
E-pinonaldehyde-A-oxide	-	0.03%	-	0.08%	-	0.01%
Z-pinonaldehyde-A-oxide	-	1.22%	-	3.15%	-	0.47%
E-pinonaldehyde-K-oxide	-	4.91%	-	12.37%	-	1.84%
Z-pinonaldehyde-K-oxide	-	12.13%	-	29.32%	-	4.20%
E-limononaldehyde-A-oxide	-	0.04%	-	0.09%	-	0.01%
Z-limononaldehyde-A-oxide	-	1.42%	-	3.67%	-	0.55%
E-limononaldehyde-K-oxide	-	2.74%	-	7.00%	-	1.06%
Z-limononaldehyde-K-oxide	-	1.70%	-	4.38%	-	0.66%

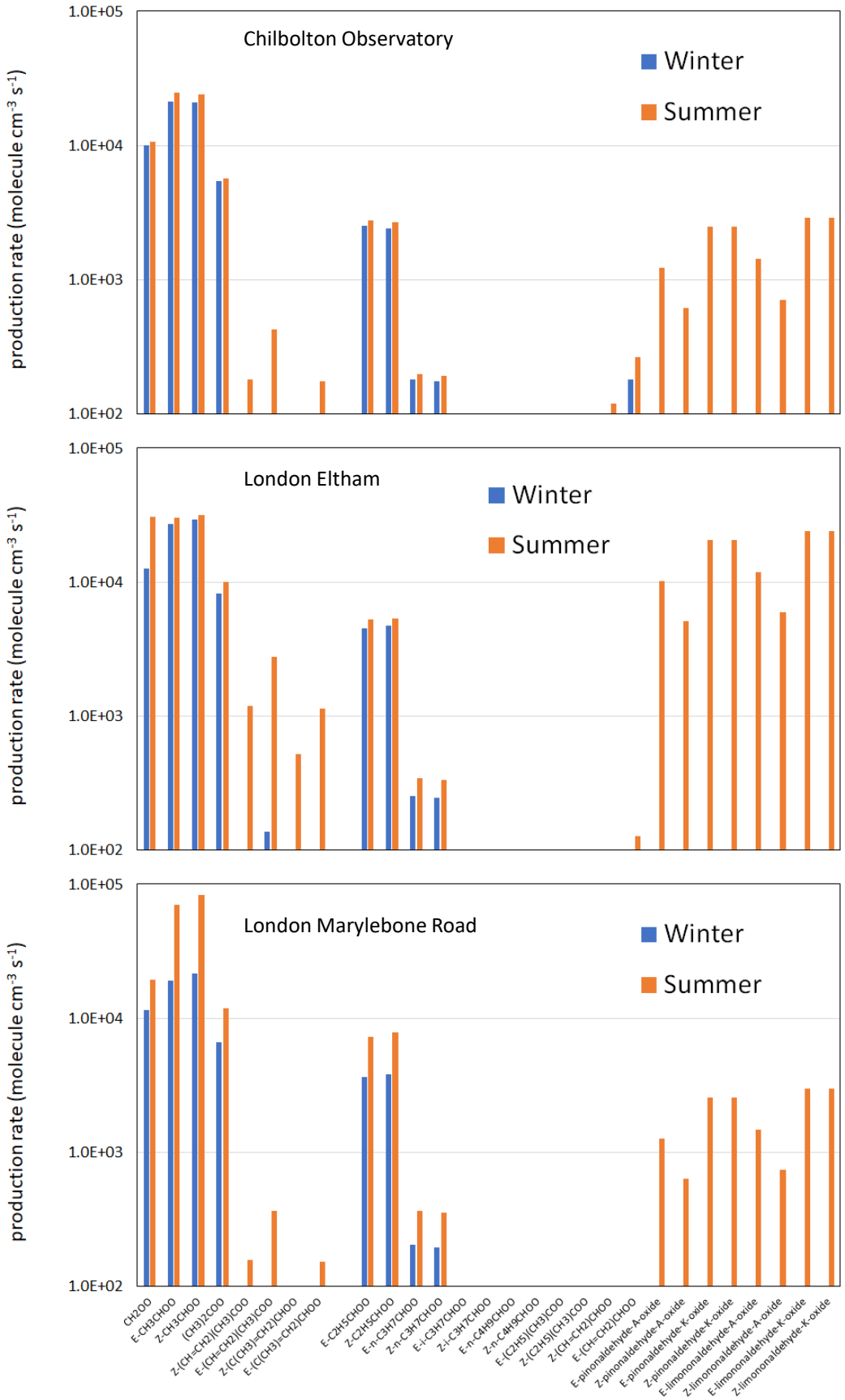

Figure 2: Production rates for the considered set of sCIs for the series of ambient conditions (summarised in Table 1). N.B. The information is presented on a log scale, with a cut-off of 10^2 molecule cm^{-3} s^{-1}. The total sCI production rates are given in Table 3.

explained by the relative abundance of trees in the locality of the three sites. The Chilbolton Observatory monitoring site is immediately surrounded by arable farmland, but with a country park (containing trees) about 400 m to the west. In contrast the London Eltham site is located in the grounds of an environmental education centre, with a mixture of trees and other vegetation in close proximity to the site. The abundance of biogenic hydrocarbons at the London Marylebone Road site has been discussed elsewhere (e.g. see pages 48-51 of AQEG, 2009). Marylebone Road is lined by *Platanus acerifolia* (London Plane) trees (e.g. Jeanjean et al., 2017), which is a high isoprene emitter (e.g. Fini et al., 2017); and Regent's Park, about 100 m to the north, contains an abundance of trees.

The sCIs formed specifically from isoprene, α-pinene and limonene therefore make increased contributions under summer conditions at all the sites. Those from α-pinene and limonene are particularly significant, because ozonolysis is generally a major (or the dominant) removal route for endocyclic alkenes, by virtue of their particularly rapid reactions with O_3. Their associated importance is therefore clearly apparent, despite the relatively low associated sCI yields from those reactions, as shown in Table 2. In contrast, the reaction of O_3 with isoprene is comparatively slow, its dominant removal reaction being with HO radicals. Therefore, the production rates of the C_4 isoprene-derived sCIs are about an order of magnitude lower than those of the monoterpene-derived sCIs under the conditions represented here.

The distribution of C_2-C_6 alkenes is consistent with road transport emissions generally being the major source, such that the abundances for most of the alkenes logically show a decreasing trend from the London Marylebone Road site through to the rural background Chilbolton Observatory site. However, it is noted that the abundances of some species (e.g. buta-1,3-diene) are elevated at the the rural site, particularly under summer conditions, and are present at higher levels than those measured at one or both London sites. Apart from a major A road about 1 km to the west of the Chilbolton Observatory site, the local roads are dominated by those in Chilbolton village (a few hundred metres to the north-west) and other rural access roads, including to the Observatory itself. In addition, there is a supplier and servicer of heavy-duty agricultural vehicles about 300 m to the north-east, and such vehicles are undoubtedly used on the surrounding arable farmland. An oil and gas supply depot is located about 1 km to the south-east of the site. The contributions of other sources may therefore account for the deviation in the hydrocarbon speciation compared with those at the London sites. The elevated buta-1,3-diene levels at the Chilbolton Observatory site result in an increased calculated abundance of the associated sCIs (i.e. *E*- and *Z*-($CH{=}CH_2$)CHOO) compared with the London sites, although the production rates are still relatively small because of the low reactivity of buta-1,3-diene with O_3.

The collective total sCI production rates for winter and summer conditions at the three locations are given in Table 3. The values range from 6.3×10^4 molecule cm^{-3} s^{-1} at the Chilbolton Observatory site in the winter to 2.4×10^5 molecule cm^{-3} s^{-1} at the London Eltham site in summer.

Loss rates: Table 3 and Figs. 3-5 present information on the speciated and total first-order loss rates of the sCIs at the three sites, and the contributions made by the series of removal reactions considered. Figs. 3 and 4 confirm that the major loss routes for most of the sCIs are either thermal decomposition, or reaction with $(H_2O)_2$ (supplemented by reaction with H_2O). As a result, these reaction classes dominate total sCI removal under all conditions (see Table 3 and Fig. 5), with reaction with $(H_2O)_2$ and H_2O being slightly more important in the winter, and thermal decomposition being slightly more important in the summer, based on the average of the three sites. In general terms, thermal decomposition tends to dominate the removal of *Z*- mono-substituted and di-substituted sCIs, with reaction with $(H_2O)_2$ and H_2O dominating the removal of *E*- mono-substituted sCIs.

The total first-order loss rates for the individual sCIs lie in approximate range 20 s^{-1} to 20,000 s^{-1} for the series of considered conditions. Those toward the low end of the range generally correspond to species for which the dominant removal route is 1,4 H atom migration, occurring at only a modest rate (e.g. as in the cases of *Z*-CH_3CHOO and *E*-($CH{=}CH_2$)(CH_3)COO), particularly under winter conditions; and for which the reactions with $(H_2O)_2$ and H_2O are very slow. Those at the high end of the range generally correspond to *E*- monosubstituted sCIs (e.g. *E*-CH_3CHOO, *E*-pinonaldehyde-A-oxide and *E*-limononaldehyde-A-oxide) for which the dominant removal reactions with $(H_2O)_2$ and H_2O are very fast. The associated loss rates for selected sCIs in the former category are sufficiently slow for removal by reaction with HC(O)OH and SO_2 (and to a lesser extent, reaction with NO_2) to make a notable contribution (see Figs. 3 and 4). In collective terms, however, these classes of reaction each makes only a small (< 4 %) contribution to total sCI removal under the conditions considered here, as shown in Table 3 and Fig. 5.

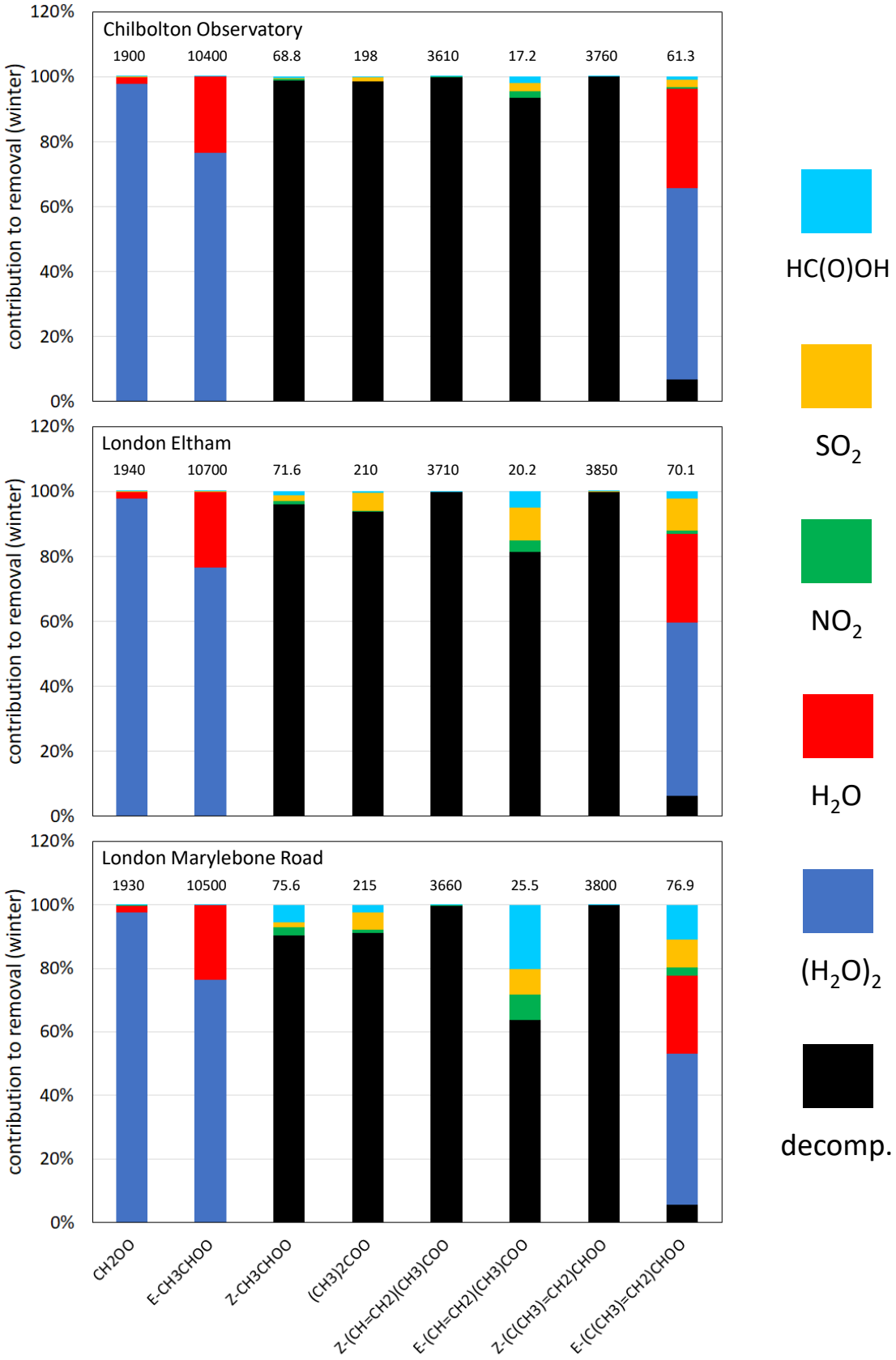

Figure 3: Contributions of the sCI unimolecular and bimolecular removal routes under winter conditions at the three locations. The data label shows the total removal rate (in s^{-1}) for the given sCI. The removal rates and contributions for the higher alkyl substituted sCIs and C_3 buta-1,3-diene derived sCIs are not shown; but are the same as for the corresponding surrogate species in the core set shown (as identified in Sect. C2).

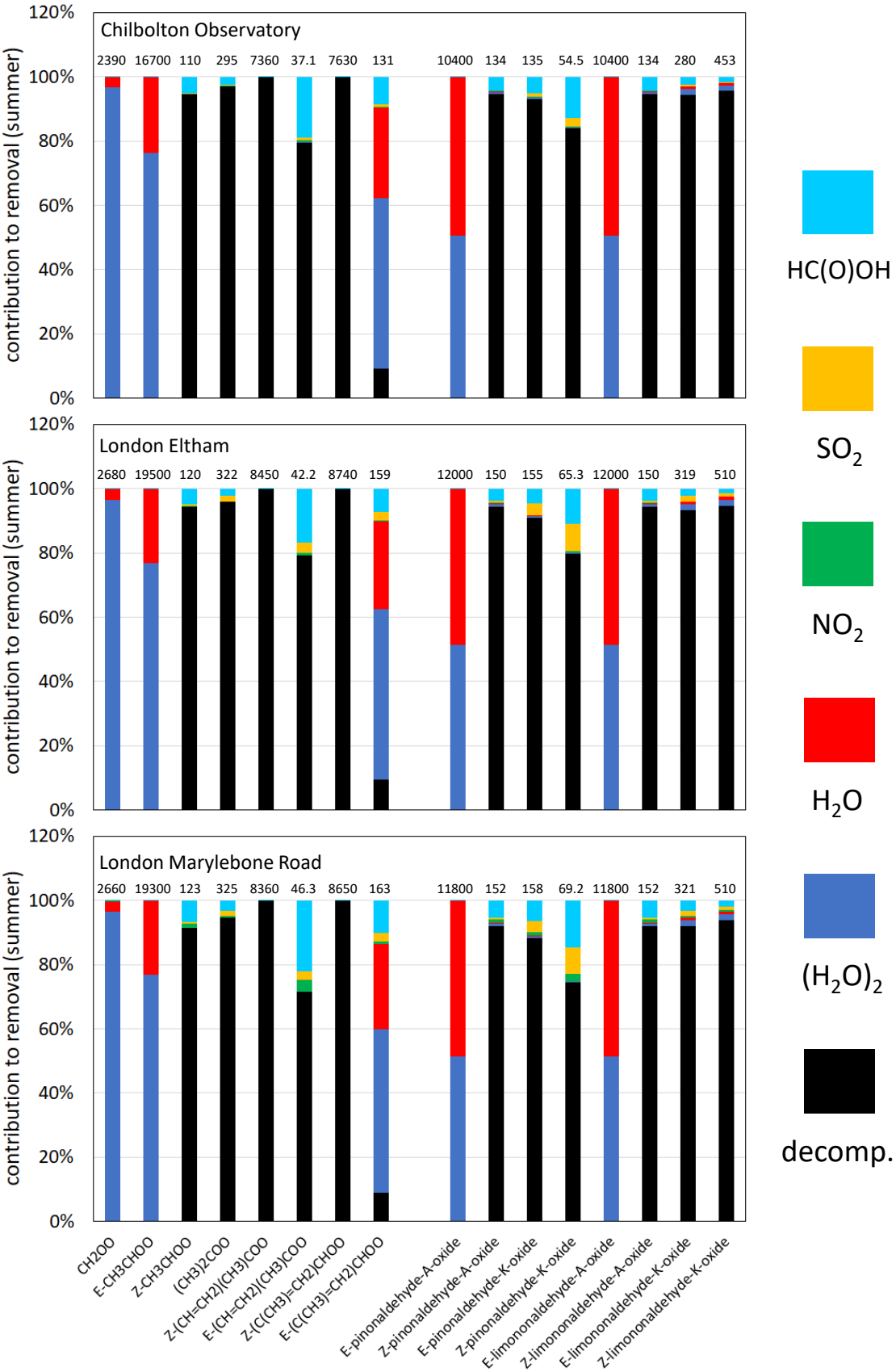

Figure 4: Contributions of the sCI unimolecular and bimolecular removal routes under summer conditions at the three locations. The data label shows the total removal rate (in s^{-1}) for the given sCI. The removal rates and contributions for the higher alkyl substituted sCIs and C_3 buta-1,3-diene derived sCIs are not shown; but are the same as for the corresponding surrogate species in the core set shown towards the left of each panel (as identified in Sect. C2).

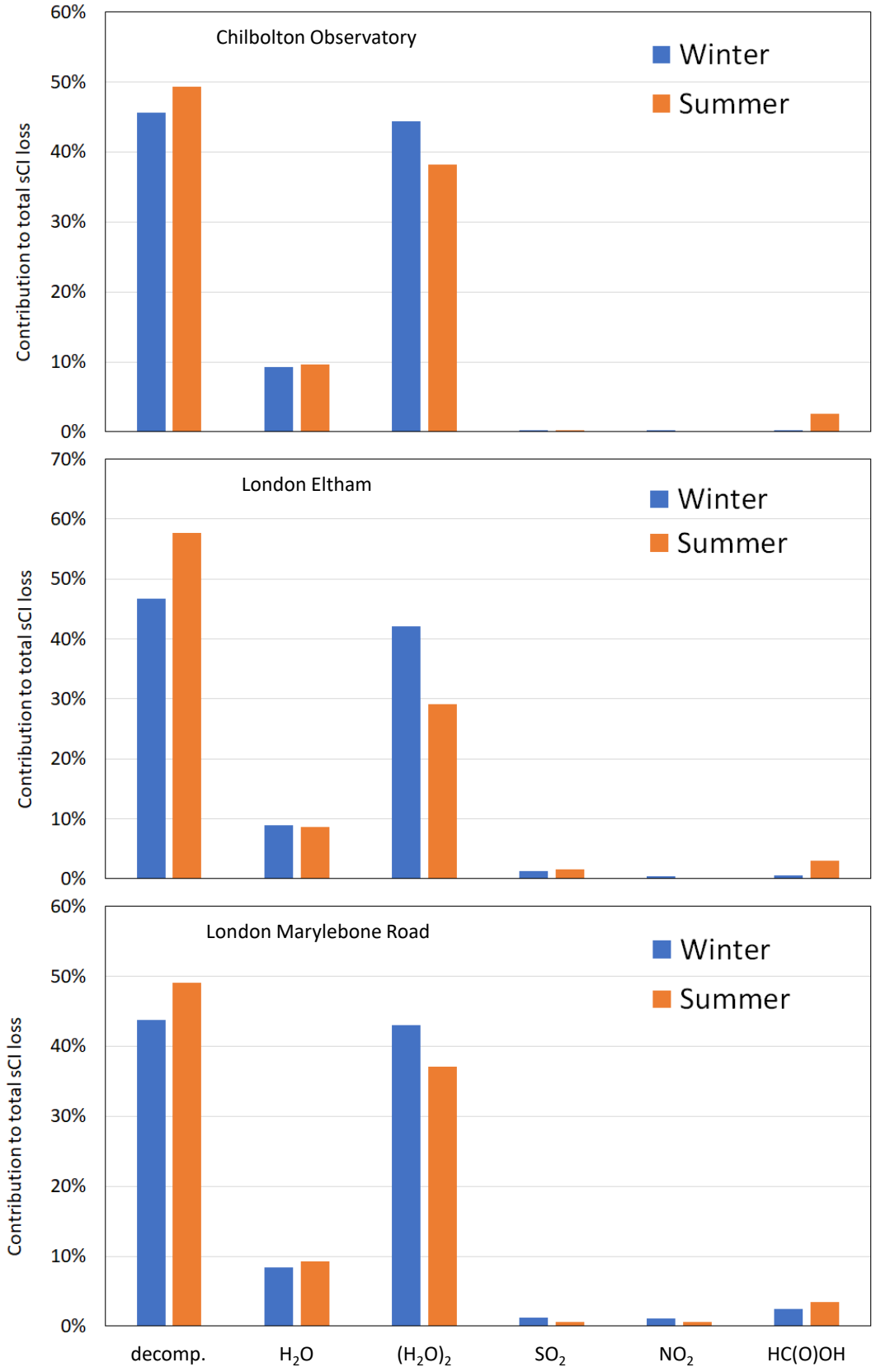

Figure 5: Contributions of the considered unimolecular and bimolecular reaction classes to the total loss of sCIs at the three locations under winter and summer conditions. This information is also presented in Table 3.

Steady-state concentrations: The total first-order sCI loss rates indicated above correspond to individual sCI lifetimes lying in the range 50 μs to 50 ms for the series of considered conditions. This confirms that calculation of their concentrations using the steady-state approximation, described by Eq. (1), is valid. The resultant calculated steady-state concentrations of the speciated sCIs for the series of ambient conditions are shown in Fig. 6, with the corresponding total sCI concentrations given in Table 3. The totals calculated for the Chilbolton Observatory rural background site (386 molecule cm^{-3} and 375 molecule cm^{-3} for winter and summer, respectively) are broadly consistent with the low annual average values simulated for the UK by Vereecken et al. (2017); and the values calculated for all the sites (see Table 3) are comparable with those reported by Khan et al. (2018), based on similar calculations to those reported here.

Fig. 6 shows that the distributions of sCIs are generally dominated by a limited series of species. Of the 28 considered sCIs, only *Z*-CH_3CHOO, $(CH_3)_2COO$ and *Z*-C_2H_5CHOO have winter concentrations greater than 10 molecule cm^{-3} at each site. This number increases to between five and eleven species for the summer conditions, mainly because of the contributions of some of the sCIs derived from the biogenic hydrocarbons, particularly at the London Eltham site. *Z*-CH_3CHOO is the most abundant sCI for all but one of the considered scenarios, accounting for 75-79 % of the total for winter conditions, and 25-77 % of the total for summer conditions. This results from the combination of its high production rate (see Fig. 2) and its relatively slow removal rate (see Fig. 4), as discussed in previous subsections. Its lowest contribution occurs for summer conditions at the London Eltham site, when the sCIs derived from α-pinene and limonene (and to a lesser extent, isoprene) are collectively dominant (67 %), with a particularly important contribution from *Z*-pinonaldehyde-K-oxide (29 %). Given the relatively low biogenic hydrocarbon emission rates in the UK, this result for a London site gives a strong indication that biogenic hydrocarbon derived sCIs will dominate the global concentrations, as clearly demonstrated in the modelling study presented by Vereecken et al. (2017). This further emphasizes the need for direct kinetics studies of a series of these structurally complex sCIs, to confirm the rate coefficients calculated in theoretical studies.

The speciated sCI distributions have also been used to calculate the associated SO_2 oxidation rates. As shown in Fig. 7 and Table 3, the total oxidation rates are calculated to be between 0.006 % h^{-1} and 0.008 % h^{-1} for the winter scenarios, and between 0.007 % h^{-1} and 0.028 % h^{-1} for the summer scenarios, and broadly follow the simulated trend in total sCI concentrations. These values can be compared with a reference SO_2 oxidation rate of about 0.3 % h^{-1} for reaction with HO radicals at a concentration of 10^6 molecule cm^{-3}. This comparison is therefore consistent with the ≤ 10 % annual average contribution to gas phase SO_2 oxidation for the UK, reported in the global modelling calculations of Vereecken et al. (2017) and Khan et al. (2018). The reactions of SO_2 with sCIs likely represents a more significant underlying route under winter and night-time conditions (when HO concentrations are low) and a less important underlying route when HO concentrations are elevated (e.g. during summertime photochemical episodes).

The speciated contributions of the sCIs to the (albeit relatively small) SO_2 oxidation rates (Fig. 7) are determined by a combination of their steady-state concentrations and the the rate coefficients for their reactions with SO_2, which vary by almost an order of magnitude. The reactions with *Z*-CH_3CHOO and $(CH_3)_2COO$ make the most important individual contributions for all the winter scenarios, accounting for 44-47 % and 39-44 % of the totals, respectively. For *Z*-CH_3CHOO, this results from its generally very high contributions to the total sCI concentration, even though its rate coefficient is at the low end of the range. For $(CH_3)_2COO$, this results from its high rate coefficient, in conjunction with modest contributions to the total sCI concentration.

The reactions with *Z*-CH_3CHOO and $(CH_3)_2COO$ make substantially reduced, but still important, contributions for the summer scenarios, accounting for 6-44 % and 5-17 % of the totals, respectively. This is because of the the generally increased concentrations of the sCIs derived from biogenic hydrocarbons, particularly at the London Eltham site. The most important contributions are made by the "K" pinonaldehyde and limononaldehyde isomers (particularly *Z*-pinonaldehyde-K-oxide), by virtue of their elevated simulated concentrations, and the rapid rate coefficients assigned to their reactions with SO_2 (by analogy with $(CH_3)_2COO$). The collective contributions of these isomers lie in the range 32-85 %, with *Z*-pinonaldehyde-K-oxide alone accounting for 17-46 %.

The more widespread potential role of biogenic hydrocarbon derived sCIs in global SO_2 oxidation has been considered in the modelling studies of Vereecken et al. (2017) and Khan et al. (2018). Although the results

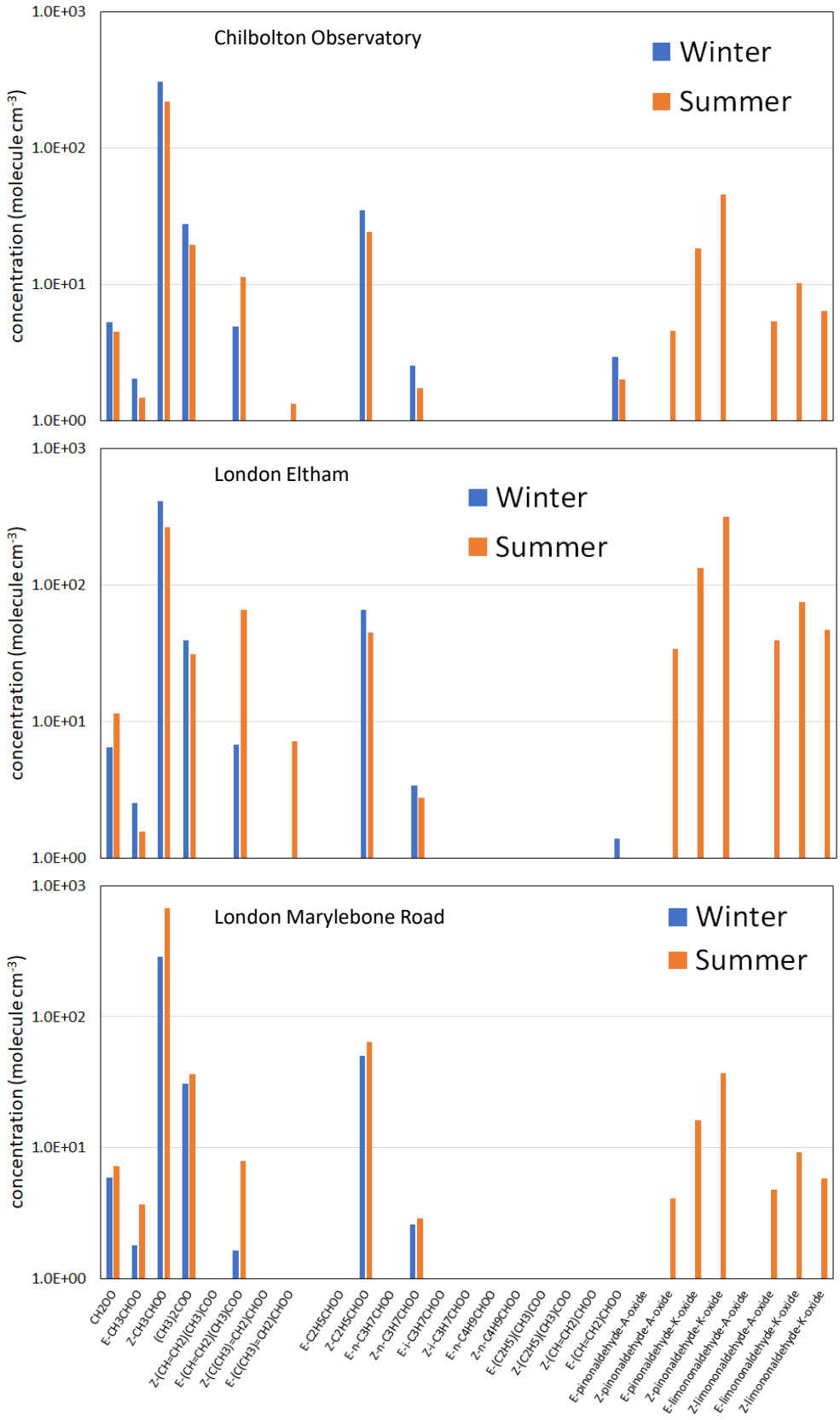

Figure 6: Calculated steady state concentrations for the considered set of sCIs for the series of ambient conditions. N.B. The information is presented on a log scale, with a cut-off of one molecule cm^{-3}. The total sCI concentrations, and speciated contributions to those totals, are given in Table 3.

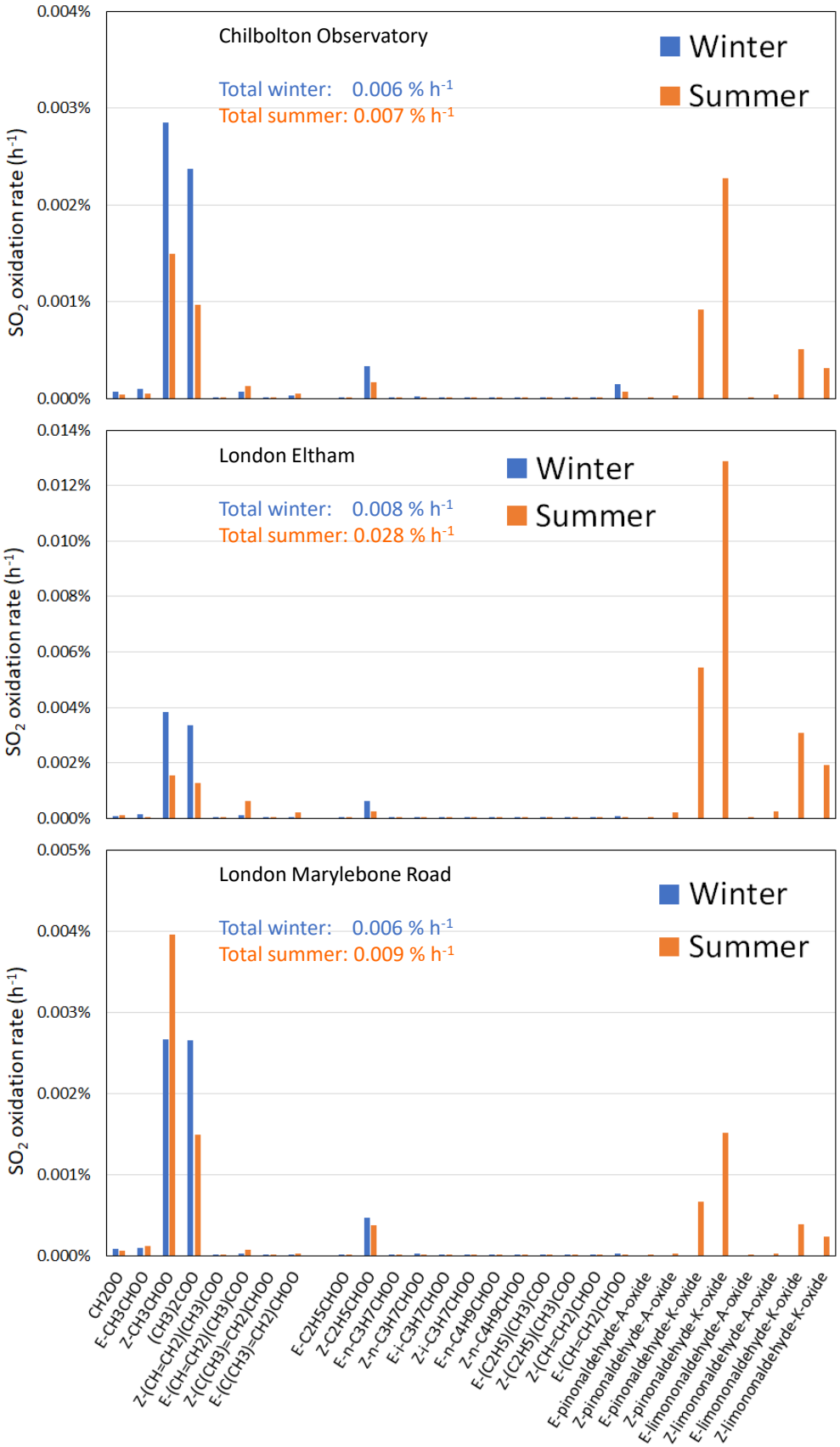

Figure 7: Contributions of the sCI distribution to the calculated SO_2 oxidation rates for the series of ambient conditions. The total SO_2 oxidation rates are also given in Table 3.

possess some similarities, their role is much more limited in the Vereecken et al. (2017) calculations, because of the high calculated decomposition rates applied to many of the sCIs (as also adopted in the present work) and the resultant suppression of sCI concentrations. This once again highlights the need for direct kinetics studies of a structurally diverse series of terpene-derived sCIs, to help validate and refine the rate coefficients calculated in theoretical studies.

The total sCI concentrations calculated here suggest associated oxidation rates of (0.04 – 0.11) % h^{-1} for HC(O)OH (see Table 3). This can be compared with a reference oxidation rate of about 0.16 % h^{-1} for reaction of HC(O)OH with HO radicals at a concentration of 10^6 molecule cm^{-3}. This indicates that reaction with sCIs makes an important contribution to HC(O)OH oxidation under the conditions considered here, with oxidation rates comparable to those via HO reaction calculated for equatorial regions in the global modelling study of Vereecken et al. (2017).

C4. Uncertainties

The calculations presented above provide estimates of the production rates, loss rates and steady-state concentrations of a series of sCIs for average ambient conditions representative of the south-east UK. Although they aim to take account of the most important production and loss routes, the estimates are inevitably subject to omissions and uncertainties in the sources and sinks of the sCIs, in addition to uncertainties associated with the kinetic parameters and sCI yields, which are discussed in the main paper and the data sheets in Supplements A and B.

As indicated in Sect. C2, the calculated production rates rely on reported ambient measurements of O_3 and alkenes, extended using emissions inventory information for C_5 and C_6 anthropogenic alkenes. Although larger alkenes are also almost certainly emitted from anthropogenic sources, it is clear that their abundances diminish systematically with increase in carbon number (as shown in Table 1), with the associated abundance of larger sCIs also decreasing substantially (as discussed in Sect. C1). However, the applied speciation of biogenically-derived terpenes was restricted to those for which measurement data are available, namely α-pinene and limonene. Although these species are expected to make an important contribution to the total terpene emissions, it is likely that additional species are also emitted. In addition, the calculations were unable to take account of the reactions of O_3 with unsaturated oxygenated products, formed particularly from the degradation of polyalkene species such as limonene. These omissions therefore contribute to factors that may result in underestimated production rates, particularly for the summer conditions.

The considered sCI loss processes include thermal decomposition and bimolecular reactions with H_2O, $(H_2O)_2$, SO_2, NO_2 and HC(O)OH, with the abundances of these species again based on, or inferred from, reported measurement data. As discussed in the main paper, this reaction set is believed to encompass the major tropospheric loss routes for sCIs. The possibility of unaccounted for reaction partners, e.g. organic acids such as $CH_3C(O)OH$ (Khan et al., 2018) and inorganic acids such as HNO_3 (Foreman et al., 2016), also contributing to sCI removal cannot be completely ruled out. However, given the small calculated contribution of reaction with HC(O)OH to sCI removal (i.e. ~3 % under summer conditions), it is likely that the collective effect of unrepresented loss reactions is much smaller than the collective effect of the processes that are represented.

Additional uncertainties are also associated with the use of averaged data. As indicated in Sect. C2, there is considerable diurnal and day-to-day variability in the abundances of O_3, alkenes and the species that react with sCIs, and also in temperature. As a result, there is also variability in the production rates, loss rates and concentrations of the sCIs. It is not straightforward to assess whether the values of these quantities based on calculations using averaged data are the same as those that would be obtained by averaging the results of many calculations using data obtained at higher temporal resolution. In particular, the abundances of O_3 and anthropogenic alkenes are likely to be anticorrelated to some extent, particularly close to road traffic sources. This results from the co-emission of nitrogen oxides (NO_x), and the well-established chemical coupling of O_3, NO and NO_2 (e.g. see Clapp and Jenkin, 2001). Use of averaged data for O_3 and anthropogenic alkenes may therefore overestimate the average production rate of the associated sCIs, particularly for the London Marylebone Road location.

References

AQEG: Ozone in the United Kingdom. Report of the UK Air Quality Expert Group, AQEG. Prepared for the Department for Environment Food and Rural Affairs, the Scottish Executive, the Welsh Assembly and the Department of the Environment in Northern Ireland. Defra publications, London, ISBN 978-0-85521-184-4, 2009.

Bannan, T. J., Murray Booth, A., Le Breton, M., Bacak, A., Muller, J. B. A., Leather, K. E., Khan, M. A. H., Lee, J. D., Dunmore, R. E., Hopkins, J. R., Fleming, Z. E., Sheps, L., Taatjes, C. A., Shallcross, D. E. and Percival, C. J.: Seasonality of formic acid (HCOOH) in London during the ClearfLo campaign, J. Geophys. Res. Atmos., 122, 12,488-12,498 https://doi.org/10.1002/2017JD027064, 2017.

Brimblecombe, P: Temporal humidity variations in the heritage climate of South East England, Herit. Sci 1, 3, https://doi.org/10.1186/2050-7445-1-3, 2013.

Clapp, L. J. and Jenkin, M. E.: Analysis of the relationship between ambient levels of O_3, NO_2 and NO as a function of NO_x in the UK, Atmos. Environ., 35, 6391-6405.

Fini A., Brunetti C., Loreto F., Centritto M., Ferrini F. and Tattini M.: Isoprene responses and functions in plants challenged by environmental pressures associated to climate change, Front. Plant Sci., 8, 1281, doi: 10.3389/fpls.2017.01281, 2017.

Foreman, E. S., Kapnas, K. M. and Murray, C.: Reactions between Criegee intermediates and the inorganic acids HCl and HNO_3: kinetics and atmospheric implications, Angew. Chem. Int. Ed., 55, 10419-10422, http://dx.doi.org/10.1002/anie.201604662, 2016.

Goodwin, J. W. L., Salway, A. G., Murrells, T. P., Dore, C. J., Passant, N. R., King, K. R., Coleman, P. J., Hobson, M. M., Pye, S. T. and Watterson, J. D.: UK Emissions of air pollutants 1970–1999. National Atmospheric Emissions Inventory Report, AEAT/ENV/R/0798. ISBN 1-85580-031 4, 2001.

Hakala, J. P. and Donahue, N. M.: Pressure stabilization of Criegee intermediates formed from symmetric trans-alkene ozonolysis, J. Phys. Chem. A, 122, 9426-9434, 2018.

Hasson, A. S., Ho, A. W., Kuwata, K. T. and Paulson, S. E.: Production of stabilized Criegee intermediates and peroxides in the gas phase ozonolysis of alkenes 2. Asymmetric and biogenic alkenes, J. Geophys. Res.-Atmos., 106, 34143-34153, 2001.

Jeanjean, A. P. R., Buccolieri, R., Eddy, J., Monks, P. S. and Leigh, R. J.: Air quality affected by trees in real street canyons: The case of Marylebone neighbourhood in central London, Urban For. Urban Green., 22, 41-53, 2017.

Khan, M. A. H., Percival, C. J., Caravan, R. L., Taatjes, C. A. and Shallcross, D. E.: Criegee intermediates and their impacts on the troposphere, Environ. Sci.: Processes Impacts, 20, 437-453, 2018.

McGillen, M. R., Carter, W. P. L., Mellouki, A., Orlando, J. J., Picquet-Varrault, B., and Wallington, T. J.: Database for the kinetics of the gas-phase atmospheric reactions of organic compounds, Earth Syst. Sci. Data Discuss., https://doi.org/10.5194/essd-2019-236, in review, 2020.

Utembe, S. R., Jenkin, M. E., Derwent, R. G., Lewis, A. C., Hopkins, J. R. and Hamilton, J. F.: Modelling the ambient distribution of organic compounds during the August 2003 ozone episode in the southern UK, Faraday Discussions 130, 311-326, 2005.

Vereecken, L., Novelli, A. and Taraborrelli, D.: Unimolecular decay strongly limits the atmospheric impact of Criegee intermediates, Phys. Chem. Chem. Phys., 19, 31599-31612, doi: 10.1039/c7cp05541b, 2017.

Whalley, L. K., Stone, D., Dunmore, R., Hamilton, J., Hopkins, J. R., Lee, J. D., Lewis, A. C., Williams, P., Kleffmann, J., Laufs, S., Woodward-Massey, R., and Heard, D. E.: Understanding in situ ozone production in the summertime through radical observations and modelling studies during the Clean air for London project (ClearfLo), Atmos. Chem. Phys., 18, 2547–2571, https://doi.org/10.5194/acp-18-2547-2018, 2018.